Optics Communications xxx (2012) xxx–xxx

Contents lists available at SciVerse ScienceDirect

Optics Communications

journal homepage: www.elsevier.com/locate/optcom

Propagation and nanofocusing of infrared surface plasmons on tapered transmission lines: Influence of the substrate

P. Sarriugarte [a], M. Schnell [a], P. Alonso-González [a], L. Arzubiaga [a], F. Golmar [a,b], F. Casanova [a,c], L.E. Hueso [a,c], R. Hillenbrand [a,c,*]

[a] CIC nanoGUNE Consolider, 20018 Donostia - San Sebastian, Basque Country, Spain
[b] I.N.T.I.-CONICET, Av. Gral. Paz 5445, Ed. 42, B1650JKA, San Martín, Bs As, Argentina
[c] IKERBASQUE, Basque Foundation for Science, 48011 Bilbao, Basque Country, Spain

ARTICLE INFO

Article history:
Received 31 October 2011
Received in revised form 1 March 2012
Accepted 2 March 2012
Available online xxxx

Keywords:
Infrared plasmonics
Nanofocusing
Transmission lines
Near-field microscopy

ABSTRACT

We study the propagation of mid-infrared surface plasmons on non-tapered and tapered two-wire transmission lines on Si and CaF_2 substrates, the two materials representing substrates with large and small refractive index, respectively. A comparative numerical study predicts a larger effective wavelength and an increased propagation length (i.e. weaker damping) for the CaF_2 substrate. By near-field microscopy we image the near-field distribution along the transmission lines and experimentally verify surface plasmon propagation. Amplitude- and phase-resolved near-field images of a non-tapered transmission line on CaF_2 reveal a standing wave pattern caused by back-reflection of the surface plasmons at the open-ended transmission line. Calculated and experimental near-field images of tapered transmission lines on Si and CaF_2 demonstrate that for both substrates the mid-IR surface plasmons are compressed when propagating along the taper. Importantly, the nanofocus at the taper apex yields a stronger local field enhancement for the low-refractive index substrate CaF_2. We assign the more efficient nanofocusing on CaF_2 to the weaker damping of the surface plasmons.

1. Introduction

Infrared light is widely used to study different material properties such as chemical composition or the structure of matter [1,2]. Infrared spectroscopy is thus an important analysis tool in materials sciences, chemistry and biology. However, conventional infrared microscopy and spectroscopy use propagating electromagnetic waves to study the samples, which limits the spatial resolution because of diffraction to about half of the wavelength, in the mid-infrared spectral range to about 5–10 μm.

In recent years it has been shown that metallic nanostructures can focus visible, infrared (IR) and terahertz (THz) radiation to nanometer-size spots (nano-focii) [3]. Acting as optical or infrared antennas, they capture free-space propagating light and convert it into localised enhanced fields, and vice versa. Optical and IR antennas have opened the door to optical imaging with nanoscale resolution [4–8], surface enhanced Raman spectroscopy (SERS) [9] of even single molecule [10–12], nanoscale IR spectroscopy [13,14], and surface enhanced IR absorption spectroscopy (SEIRA) [15,16].

An alternative concept for nanofocusing of light is based on adiabatic compression of surface plasmon polaritons. Such a compression is achieved when the surface plasmon propagates along tapered metal wires [17–26] or along tapered slot waveguides [27–31], yielding a strongly concentrated field at the taper apex. Recently, we succeeded to nanofocus mid-IR surface plasmons with tapered two-wire transmission lines [32]. The propagation length of mid-IR surface plasmons on two-wire (coplanar strip) transmission lines [33] was observed to be in the range of 10 μm, which is in the order of the free-space wavelength [32,34]. Such relatively short propagation lengths challenge the development of mid-IR nanophotonics and may limit the maximum field enhancement at the apex of tapered transmission lines. On the other hand, the reported mid-infrared transmission lines were fabricated on Si substrates, which have a rather large refractive index, $n_{Si} > 3$ at mid-IR wavelengths [35]. It is well known that substrates with a large refractive index strongly affect the near-field enhancement and damping of surface plasmon polaritons [36]. Here we study the influence of the substrate on the propagation of mid-IR surface plasmons on two-wire transmission lines. Particularly, we compare the performance of tapered transmission lines on Si and CaF_2 substrates, the latter exhibiting a much lower refractive index of $n_{CaF2} \approx 1.3$ [35] at 9.3 μm wavelength. To this end, we fabricated two-wire transmission lines on a CaF_2 substrate, image their IR near-field distribution and compare the results with recently published data [32] obtained for transmission lines on Si.

* Corresponding author at: CIC nanoGUNE Consolider, 20018 Donostia - San Sebastian, Basque Country, Spain. Tel.: +34 943 57 4007; fax: +34 943 574 001.
E-mail address: r.hillenbrand@nanogune.eu (R. Hillenbrand).

0030-4018/$ – see front matter © 2012 Elsevier B.V. All rights reserved.
doi:10.1016/j.optcom.2012.03.004

2. Numerical studies of mid-IR transmission lines

Fig. 1a shows the cross section of a typical two-wire transmission line on a dielectric substrate, which consists of two infinitely long parallel metallic wires. We define the total width of the transmission line by $W=2w+g$, where w is the width of the metal wires and g the distance between them. In Fig. 1b we show the calculated mode profiles (intensity) for two-wire transmission lines on a CaF_2 substrate for different widths W. The calculations were performed with a commercial mode solver (www.lumerical.com). From the set of solutions we have selected the antisymmetric mode, where the fields on the parallel wires oscillate 180° out of phase (illustrated by + and − signs in Fig. 1b). As we show later in Fig. 4, this mode is the one that is excited and propagates along the transmission line by attaching a dipole antenna to it [37]. For all calculations we assume a free-space wavelength of $\lambda=9.3\,\mu m$ and use the dielectric values for Au and CaF_2 from Palik [35] ($\varepsilon_{Au}=-2591+1145i$; $\varepsilon_{CaF2}=1.74$). We find that the near fields associated to the modes are strongly confined on the scale of the transmission-line width W, even for the narrowest case C with $W=90$ nm ($\lambda/100$). Similar field confinements have been reported for transmission lines on Si [32,34].

In order to compare the performance of transmission lines on the two different substrates, CaF_2 and Si, we display in Fig. 2a the effective wavelength λ_{eff} and in Fig. 2b the propagation length L as a function of the total width $W=2w+g$, where the gap width g increases linearly from 50 nm to 300 nm and the wire width from $w=20$ nm to 200 nm. Following our previous work on near-field mapping of transmission lines [32], we define the propagation length L as the distance

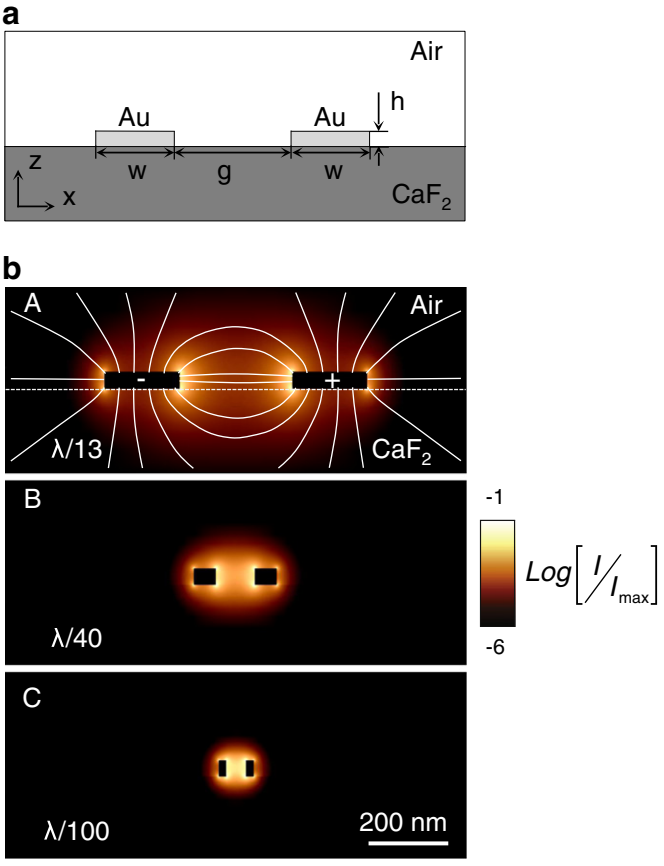

Fig. 1. Two-wire transmission lines on a CaF_2 substrate. a) Schematics of the cross section. b) Numerically calculated mode profiles which are excited at $\lambda=9.3\,\mu m$ wavelength. Mode profiles are plotted for three situations A, B and C, in which the total width ($W=2w+g$) is 700 nm, 212 nm and 90 nm, respectively. The mode profiles are normalized to their maximum value.

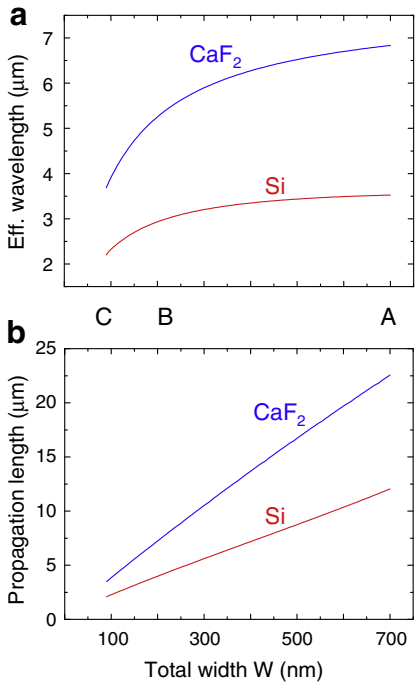

Fig. 2. Propagation properties of surface plasmon modes on two-wire transmission lines of total width W. a) Effective wavelength λ_{eff}. b) Propagation length L as a function of the total transmission line width ($W=2w+g$) on CaF_2 (blue curves) and on Si (red curves) substrates, while the wire width t and the gap size g are decreased simultaneously from $w=200$ nm to 20 nm and $g=300$ nm to 50 nm. The letters A, B and C indicate the transmission lines shown in Fig. 1b. (For interpretation of the references to color in this figure legend, the reader is referred to the web version of this article.)

where the field amplitude decays by a factor of 1/e. For both the CaF_2 (blue curves) and Si (red curves) substrate the effective wavelength λ_{eff} decreases when the width W of the transmission line is reduced, as the overlap between the surface plasmon's modal profile and the metal increases [31]. We also see that λ_{eff} is larger by about a factor of two on the transmission lines on CaF_2. This can be explained essentially by the lower refractive index of the CaF_2 substrate. When considering the transmission line being embedded in a homogeneous medium with an effective refractive index $n_{eff}=\varepsilon_{eff}^{1/2}=[(\varepsilon_{air}+\varepsilon_{subs})/2]^{1/2}$ [38], we obtain $n_{eff,Si}=2.28$ for the transmission line on Si and $n_{eff,CaF2}=1.17$ for the transmission line on CaF_2. The effective refractive index for CaF_2 is thus half as large as the one for Si, which explains why the effective wavelength on Si is a factor of two smaller.

We find that on both substrates the propagation length L decreases for smaller W. This can be attributed to the increasing amount of energy propagating inside the gold (skin depth effect) [32,39], yielding damping of the surface plasmons because of the losses inside the metal. Furthermore, the propagation length L is about a factor of two smaller on the transmission lines on Si. The higher refractive index of Si makes the optical field to be more confined, increasing the field magnitude at the Au-Si interface (and inside the gold) and thus resulting in a greater absorption loss [36,40]. Our numerical study thus suggests to employ low refractive index materials for the development of mid-IR transmission lines, particularly for nanofocusing mid-IR light in tapered transmission lines as we show later in Fig. 5.

3. Near-field microscopy of mid-IR transmission lines

We experimentally study two-wire transmission lines on a CaF_2 substrate by imaging their near-field distribution with a scattering-type Scanning Near-Field Optical Microscope (s-SNOM) [5]. In order to launch a surface plasmon (Fig. 1b) on the transmission line, a dipole

Please cite this article as: P. Sarriugarte, et al., Propagation and nanofocusing of infrared surface plasmons on tapered transmission lines: Influence of the substrate, Opt. Commun. (2012), doi:10.1016/j.optcom.2012.03.004

antenna is attached to the left end of the transmission line [32,34]. Fig. 3a illustrates the imaging principle. A conventional, cantilevered silicon (Si) tip is used as a near-field probe, scanning the transmission line. The tip apex scatters the local near field of the IR surface plasmons [32,34,41,42] (illustrated schematically by red curved lines over the transmission line), which is subsequently detected by a distant detector in the far field. The transmission line is illuminated from below through the transparent substrate (transmission-mode s-SNOM [32,43]), with a polarization parallel to the dipole antenna. This way the antenna is efficiently excited and launches a surface plasmon on the transmission line. The tip, in contrast, is only weakly polarized, which prevents disturbance of the near-field distribution of the transmission line [43–46]. Transmission-mode s-SNOM has been already used successfully to image the mid-IR near-field distributions of infrared antennas and transmission lines on Si substrates [32,43,47,48].

Further details of the setup used in this work are shown in Fig. 3b. A CO_2 laser tuned at a wavelength $\lambda = 9.3$ μm is weakly focused to the sample through a low-numerical aperture objective, yielding a mid-IR spot of about 50 μm in diameter for the purpose of homogeneous sample illumination. The light scattered by the tip is collected with a parabolic mirror at an angle of about 60° normal to the sample surface. The collected light is interfered with a reference beam at the detector. Because of the global sample illumination, the collected light contains a large amount of background. In the presented experiments this background contributions could be fully suppressed by vertical tip oscillation at a frequency Ω (about 300 kHz) and subsequent higher harmonic demodulation of the detector signal at 3Ω, which is the typical procedure for background suppression in s-SNOM [5,49]. In order to visualize the propagation of electromagnetic modes, we map both amplitude and phase of the near-field distribution. To this end, the tip-scattered light is detected with a pseudo-heterodyne Mach–Zehnder interferometer [49]. The reference mirror is oscillating at a frequency M (~600 Hz), in order to modulate the phase of the reference beam, which is vertically polarized (Fig. 3b). Thus, by demodulating the detector signal at frequencies $M + 3\Omega$ and $2M + 3\Omega$, both amplitude $|E_z|$ and phase φ_z images of the vertical (z) near-field component can be recorded simultaneously to the topography [32,43,47,48].

4. Fabrication of mid-IR transmission lines on a CaF_2 substrate

The two-wire transmission lines were fabricated by high-resolution e-beam lithography and metal lift-off. A bilayer of polymethyl methacrylate (with molecular weight of 495 kDa at the bottom and 950 kDa at the top) was used as electron-sensitive polymer. Because CaF_2 is an insulator, the surface of the substrate is charged when exposed to the electron beam, which can deviate the beam. In order to avoid charging of the sample, a 1.5 nm thick gold layer was sputtered on top of the electron-sensitive polymer. After the electron beam exposure the sputtered gold layer was etched with a solution of KI_3 ($KI + I_2$). The sample was then developed in methyl isobutyl ketone (MIBK) and isopropanol alcohol (IPA) at a ratio of 1:3. Then a 40 nm gold film was thermally evaporated in high vacuum on top of 3 nm thick titanium layer, which before was electron beam evaporated onto the CaF_2 substrate for adhesion purposes. Finally, a lift-off was done by immersion of the sample in acetone for about 4 hours, followed by about 15 s of ultrasound treatment and IPA rinse.

5. Experimental verification of mid-IR transmission lines on a CaF_2 substrate

We first verify the propagation of surface plasmons on a 6 μm long two-wire transmission line on CaF_2, which has a total width of $W = 700$ nm (cross section A in Fig. 1b). Fig. 4a shows the topography image of the transmission line and the dipole antenna attached at its left end. The amplitude $|E_z|$ and phase φ_z images of the vertical near-field component are shown in Fig. 4c. We observe strong near-field amplitude signals on the parallel metal wires, which prove that the antenna couples an IR mode into the subwavelength-scale transmission line. The 180° phase jump between the two wires proves that the mode is antisymmetric, i.e. the near fields on the two parallel wires oscillate in antiphase as indicated by the plus and minus signs in the phase image. We also observe amplitude maxima and minima along the parallel wires. They reveal a standing wave pattern, which is confirmed by the phase jumps of 180° along the wires. The standing wave pattern on the transmission line is generated because of the back-reflection at the right open end of the transmission line, where the wave finds an impedance mismatch [34]. We measure that the distance between the minima is about 3.5 μm, which is the half of the effective wavelength of the IR mode, $\lambda_{eff}/2$. This is in excellent agreement with the theoretically expected wavelength $\lambda_{eff} = 7$ μm (see position A in Fig. 2a). For comparison we performed numerical calculations with a commercial software package (www.lumerical.com). We consider a homogenous plane wave illumination from below. In Fig. 4d we show the vertical near-field component at 30 nm above the transmission line. We see that our experimental results are well reproduced by numerical calculations.

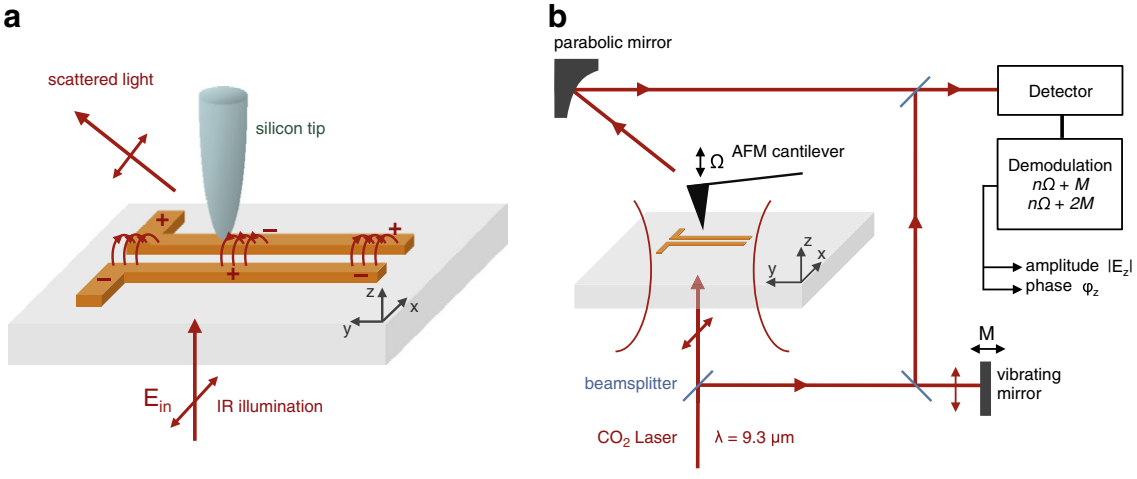

Fig. 3. a) Principle of transmission-mode s-SNOM. A silicon tip is scattering the near-fields from the transmission line that is illuminated from below through the substrate with polarization parallel to the dipolar antenna. The scattered light is collected above the surface in y-direction at an angle of about 60° normal to the surface. b) Schematics of the transmission-mode s-SNOM. The near field scattered by the silicon tip is detected with a pseudo-heterodyne interferometer, yielding amplitude and phase images of the vertical field component.

Please cite this article as: P. Sarriugarte, et al., Propagation and nanofocusing of infrared surface plasmons on tapered transmission lines: Influence of the substrate, Opt. Commun. (2012), doi:10.1016/j.optcom.2012.03.004

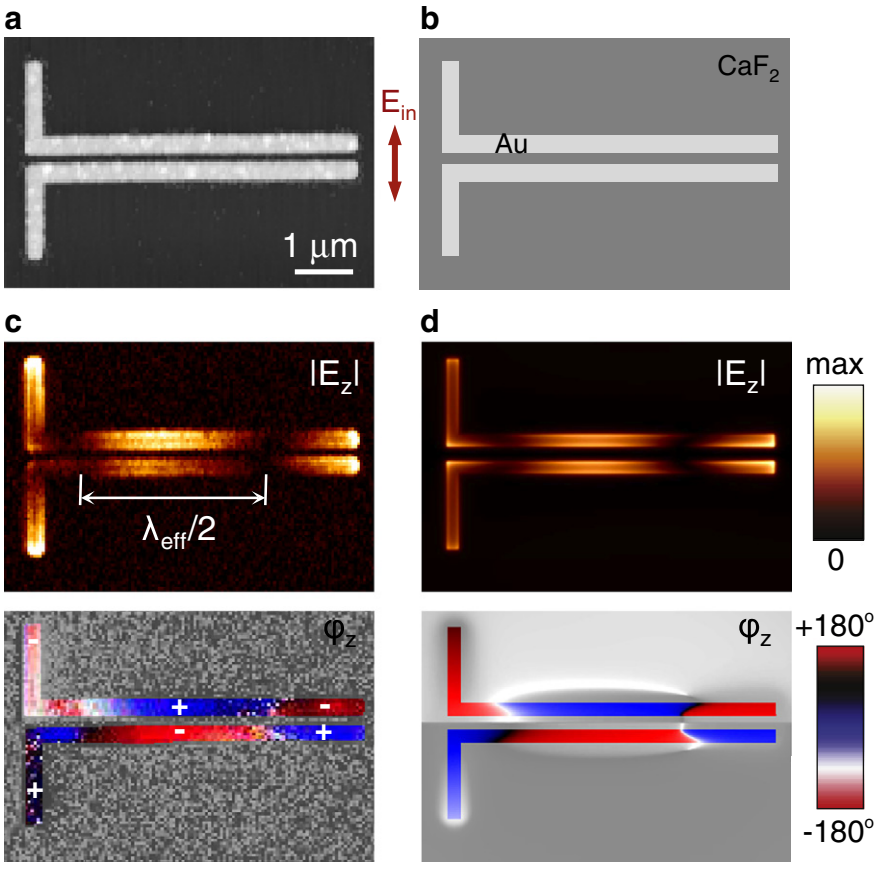

Fig. 4. Near-field images of a two-wire transmission line. a) AFM topography. b) Geometry used for numerical calculations. c) Experimental near-field images showing amplitude $|E_z|$ (top) and phase φ_z (bottom) of the vertical near-field component. d) Numerically calculated near-field images showing amplitude $|E_z|$ (top) and phase φ_z (bottom) of the vertical near-field component 30 nm above the transmission lines. The phase images are displayed in a cyclic colour scale where white colour represents $-90°$, blue 0°, black 90° and red $\pm 180°$.

6. Comparative study of mid-IR nanofocusing with tapered transmission lines on Si and CaF_2 substrates

In Fig. 5 we compare experimentally and numerically the nanofocusing capabilities of tapered transmission lines on CaF_2 and Si substrates. To that end we imaged and calculated the near-field distribution of a 6 μm long tapered transmission line on CaF_2 substrate (Fig. 5a) and compare it with the results obtained for a transmission line of the same geometry on Si (Fig. 5b, numerical and experimental data taken from ref [32]). As seen in the topography images (Fig. 5a and b, top), we tapered the right open end of the transmission lines over a length of 1 μm by reducing the total width *W* of the transmission line linearly form 700 nm (case A in Fig. 1b) to 90 nm (case C in Fig. 1b). Both transmission lines were imaged with our transmission-mode s-SNOM [43] at a wavelength of $\lambda = 9.3$ μm. The experimental (Fig. 5a and b, middle) and calculated (Fig. 5a and b, bottom) near-field images show the intensity of the vertical near-field component I_z. Similar to the untapered transmission in Fig. 4, we see one interference maximum in the middle of the transmission line on CaF_2 (Fig. 5b), which is caused by a back-reflection of the surface plasmons at the open-ended taper. On the transmission line on Si (Fig. 5b) we observe two fringes along the untapered part of the transmission line, as the surface plasmon wavelength is reduced by a factor of two (see Fig. 2). More importantly, on both transmission lines we see a significant increase of the near-field intensity towards the taper apex, which is caused by the compression of the surface plasmons when they propagate along the taper [32]. We note that a similar intensity increase occurs for the in-plane (x) near-field component, exhibiting its maximum inside gap at the taper apex [32]. However, the near-field signal of the x-component was much weaker and below the noise level on the untapered part of the transmission lines. In the following, we thus use the z-component for evaluating and comparing the intensity enhancement at the taper apices.

In order to compare the intensities I_{max} at the taper apices, we normalized the intensity of the vertical near-field component I_z to the value I_z^{ref} measured at the first interference maximum before the taper, in both experimental and calculated images, and for both substrates. On CaF_2 we find an intensity enhancement $I_z^{max}/I_z^{ref} \approx 14$ in the experiment and $I_z^{max}/I_z^{ref} \approx 17$ in the calculation. In the case of the Si substrate, we obtain $I_z^{max}/I_z^{ref} \approx 4$ in both the experiment and the calculation. The intensity enhancement is thus clearly stronger on the CaF_2 substrate, by about a factor of 4. The quantitative discrepancies between experiment and theory we attribute to fabrication uncertainties particularly at the taper apex. We explain the stronger field enhancement at the taper apex on the CaF_2 substrate to the larger propagation length, i.e. reduced losses of the surface plasmons.

7. Conclusions

In conclusion, we showed that the propagation length of mid-infrared surface plasmons on two-wire transmission lines is about twice as long on CaF_2 substrates compared to Si substrates. The stronger damping of the surface plasmons on the Si substrate is explained by the enhanced interaction between the electromagnetic fields and the lossy metal. We also found that the reduced losses on CaF_2 substrates yield a stronger field enhancement at the apex of tapered transmission lines. The use of CaF_2 substrates or other low refractive index materials will thus allow for more efficient nanofocusing of

Please cite this article as: P. Sarriugarte, et al., Propagation and nanofocusing of infrared surface plasmons on tapered transmission lines: Influence of the substrate, Opt. Commun. (2012), doi:10.1016/j.optcom.2012.03.004

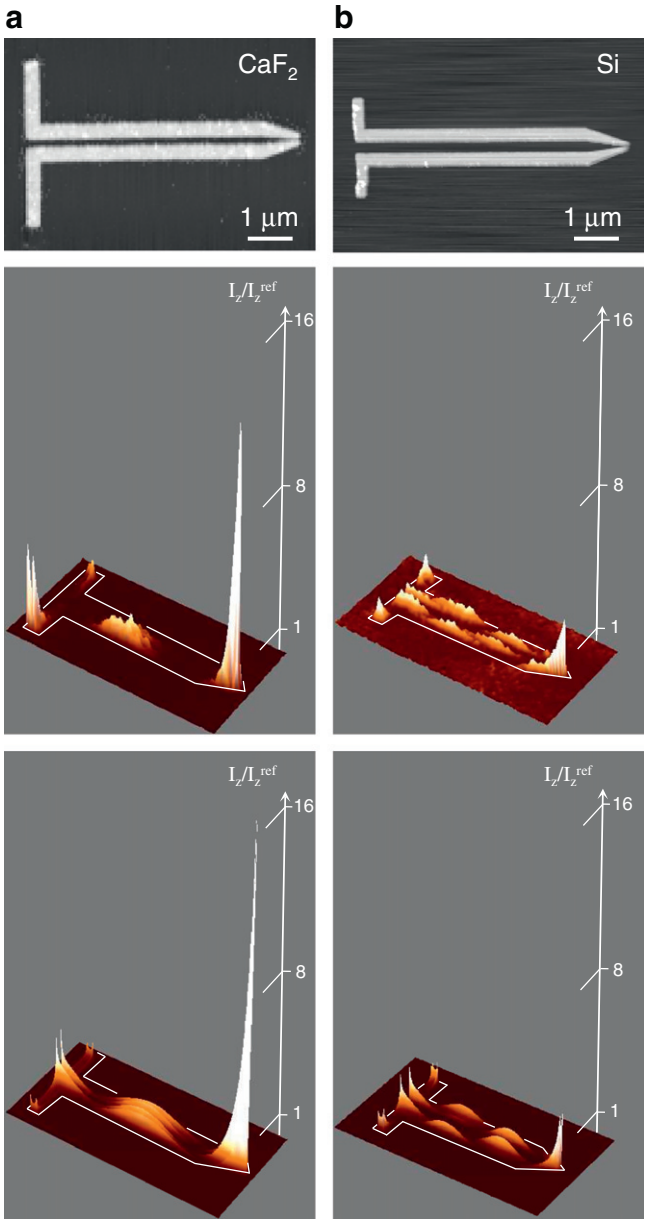

Fig. 5. a) Topography image of a tapered transmission line on CaF_2 (top). Experimental (middle) and numerically calculated (bottom) near-field images showing the intensity of the vertical field component, I_z. b) Topography image of a tapered transmission line on Si (top). Experimental (middle) and numerically calculated (bottom) near-field images showing the intensity of the vertical field component, I_z (data taken from ref. [32]).

mid-IR light, which will be beneficial for the development of integrated mid-IR sensors and near-field probes.

Acknowledgements

Supported by the European FP7 project "Nanoantenna" (FP7-HEALTH-F5- 2009-241818-NANOANTENNA) and the National Projects MAT2009-08398 and MAT2009-08494 from the Spanish Ministerio de Ciencia e Innovacion. P.S., M.S. and L.A. acknowledge the financial support from "Ikertzaileen Prestakuntza eta Hobekuntzarako Programa" promoted by the Department of Education, Universities and Research of the Basque Government.

References

[1] A. Gutberlet, et al., Science 324 (2009) 1545.
[2] Z.Q. Li, et al., Nature Physics 4 (2008) 532.
[3] J.A. Schuller, et al., Nature Materials 9 (2010) 193.
[4] P. Mühlschlegel, H.-J. Eisler, O.J.F. Martin, B. Hecht, D.W. Pohl, Science 308 (2005) 1607.
[5] F. Keilmann, R. Hillenbrand, Philosophical Transactions of the Royal Society of London. Series A 362 (2004) 787.
[6] L. Novotny, Physical Review Letters 98 (2007) 266802.
[7] S. Kühn, U. Hakanson, L. Rogobete, V. Sandoghdar, Physical Review Letters 97 (2006) 017402.
[8] T.H. Taminiau, F.D. Stefani, F.B. Segerink, N.F. Van Hulst, Nature Photonics 2 (2008) 234.
[9] M. Moskovits, Reviews of Modern Physics 57 (1985) 783.
[10] H. Xu, E.J. Bjerneld, M. Käll, L. Börjesson, Physical Review Letters 83 (1999) 4357.
[11] S. Nie, S.R. Emory, Science 275 (1997) 1102.
[12] K. Kneipp, et al., Physical Review Letters 78 (1997) 1667.
[13] F. Huth, M. Schnell, J. Wittborn, N. Ocelic, R. Hillenbrand, Nature Materials 10 (2011) 352.
[14] S. Amarie, F. Keilmann, Physical Review B 83 (2011) 045404.
[15] F. Neubrech, et al., Physical Review Letters 101 (2008) 157403.
[16] A.A. Yanik, et al., Proceedings of the National Academy of Sciences of the United States of America 108 (2011) 11784.
[17] L. Novotny, C. Hafner, Physical Review E 50 (1994) 4094.
[18] J. Takahara, S. Yamagishi, H. Taki, A. Morimoto, T. Kobayashi, Optics Letters 22 (1997) 475.
[19] F. Keilmann, Journal of Microscopy 194 (1999) 567.
[20] M.I. Stockman, Physical Review Letters 93 (2004) 137404.
[21] E. Verhagen, M. Spasenovicacute, A. Polman, L. Kuipers, Physical Review Letters 102 (2009) 203904.
[22] F. De Angelis, et al., Nature Nanotechnology 5 (2010) 67.
[23] C. Ropers, et al., Nano Letters 7 (2007) 2784.
[24] C.C. Neacsu, et al., Nano Letters 10 (2010) 592.
[25] K. Wang, D.M. Mittleman, Nature 432 (2004) 376.
[26] T. Akalin, A. Treizebre, B. Bocquet, IEEE Transactions on Microwave Theory and Techniques 54 (2006) 2762.
[27] D.F.P. Pile, D.K. Gramotnev, Applied Physics Letters 89 (2006) 041111.
[28] H. Choi, D.F. Pile, S. Nam, G. Bartal, X. Zhang, Optics Express 17 (2009) 7519.
[29] S. Vedantam, et al., Nano Letters 9 (2009) 3447.
[30] H. Zhan, R. Mendis, D.M. Mittleman, Optics Express 18 (2010) 9643.
[31] W. Cai, W. Shin, S. Fan, M.L. Brongersma, Advanced Materials 22 (2010) 5120.
[32] M. Schnell, et al., Nature Photonics 5 (2011) 283.
[33] T. Mandviwala, B. Lail, G. Boreman, Microwave and Optical Technology Letters 47 (2005) 17.
[34] P.M. Krenz, R.L. Olmon, B.A. Lail, M.B. Raschke, G.D. Boreman, Optics Express 18 (2010) 21678.
[35] E.D. Palik, Handbook of Optical Constants of Solids, Academic Press, 1985.
[36] H. Raether, Surface plasmons on smooth and rough surfaces and on gratings, vol. 111, Springer, 1988.
[37] J.-S. Huang, T. Feichtner, P. Biagioni, B. Hecht, Nano Letters 9 (2009) 1897.
[38] F. Neubrech, et al., Applied Physics Letters 89 (2006) 253104.
[39] A. Rusina, M. Durach, K.A. Nelson, M.I. Stockman, Optics Express 16 (2008) 18576.
[40] T. Holmgaard, S.I. Bozhevolnyi, Physical Review B 75 (2007).
[41] A. Babuty, et al., Physical Review Letters 104 (2010).
[42] J.P. Tetienne, et al., Applied Physics Letters 97 (2010).
[43] M. Schnell, et al., Journal of Physical Chemistry C 114 (2010) 7341.
[44] R.L. Olmon, P.M. Krenz, A.C. Jones, G.D. Boreman, M.B. Raschke, Optics Express 16 (2008) 20295.
[45] A.C. Jones, et al., Nano Letters 9 (2009) 2553.
[46] R. Esteban, et al., Nano Letters 8 (2008) 3155.
[47] M. Schnell, A. Garcia-Etxarri, J. Alkorta, J. Aizpurua, R. Hillenbrand, Nano Letters 10 (2010) 3524.
[48] M. Schnell, et al., Nature Photonics 3 (2009) 287.
[49] N. Ocelic, A. Huber, R. Hillenbrand, Applied Physics Letters 89 (2006) 101124.

Please cite this article as: P. Sarriugarte, et al., Propagation and nanofocusing of infrared surface plasmons on tapered transmission lines: Influence of the substrate, Opt. Commun. (2012), doi:10.1016/j.optcom.2012.03.004